Adv. Space Res. 73, 4539-4545, 2024. doi:10.1016/j.asr.2024.02.011

Ionospheric changes immediately before the 2008 Wenchuan earthquake

*Kosuke Heki[(1),(2)], Masao Nakatani[(3)], & Wei Zhan[(4)]

(1) Shanghai Astr. Obs., Chinese Acad. Sci., 80 Nandan Rd., Shanghai 200030, China
(2) Hokkaido Univ., N10 W8, Kita-ku, Sapporo, Japan; e-mail: heki@sci.hokudai.ac.jp
(3) Earthq. Res. Inst., Univ. Tokyo, Yayoi 1-1-1, Bunkyo-ku, Tokyo, Japan
(4) First Monitoring and Application Center, China Earthq. Admin., Tianjin, China
*corresponding author, Kosuke Heki, email:heki@sci.hokudai.ac.jp

Abstract

Ionospheric disturbances associated with large earthquakes can be observed with global navigation satellite system (GNSS) receivers on the ground as changes in total electron content (TEC). In addition to coseismic disturbances ~10 minutes after earthquakes caused by acoustic-gravity waves from epicenters, there have been reports on changes immediately before very large earthquakes. We show such disturbances for the 2008 Wenchuan earthquake (M_w7.9), China, started ~37 minutes before the main shock and reached ~5 percent of the background value. The results of past ~20 cases with M_w 7.3 or more exhibit simple relationships that the leading times scale with fault lengths and the intensities of the anomalies relative to the backgrounds scale with fault areas. We demonstrate that the anomaly immediately before the 2008 Wenchuan earthquake fits well with these trends but with slightly longer leading time and stronger intensity.

Highlights

GNSS-TEC data showed ionospheric changes immediately before the 2008 M_w7.9 Wenchuan earthquake, China

TEC trend showed positive changes in trends ~1/2 hour before the earthquake and the anomaly reached ~5 % of the background

These anomalies are mostly consistent with worldwide trends of past examples for ~20 earthquakes

Keywords
GNSS-TEC; 2008 Wenchuan earthquake; Precursors; Scaling law

1. Introduction

The 2008 May 12 Wenchuan earthquake (M_w7.9) occurred in the eastern margin of the Tibetan Plateau, along the fault running along the northwestern limb of the Sichuan Basin, China (Fig.1a). The ruptured fault, the central part of the Longmen Shan fault, strikes NE-SW and extends for ~300 km (Xu et al., 2009). The rupture started at its southwestern end, and propagated northeastward, with the fault mechanism showing thrust and right-lateral components. There were continuous global navigation satellite system (GNSS) receiving stations around the fault. Although many receivers within the Sichuan Basin stopped recording by the earthquake, significant number of stations in the west highland area continued recording valuable data.

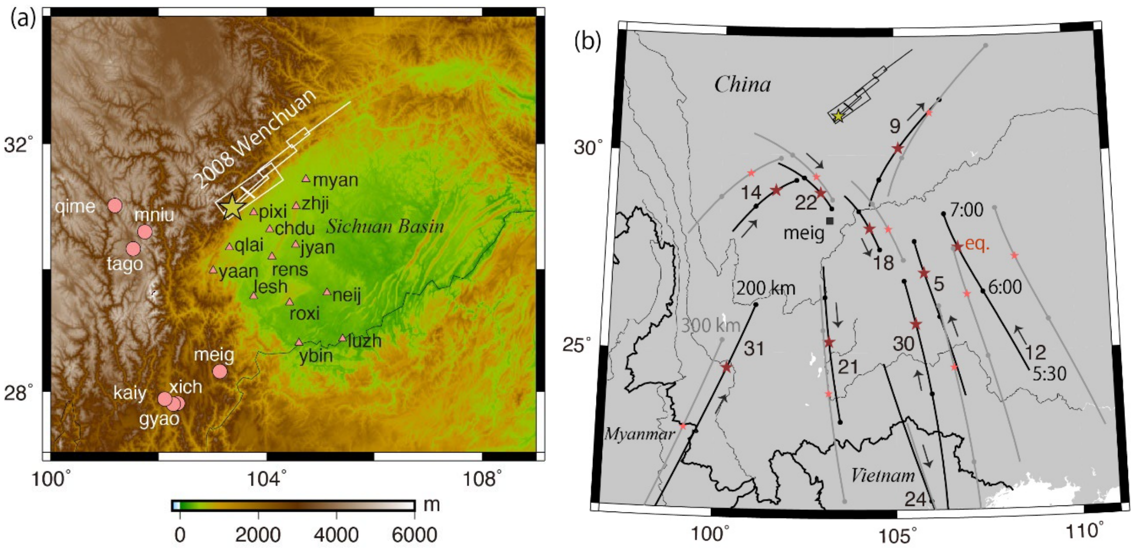

Fig. 1. (a) Continuous GNSS stations around the faults of the 2008 Wenchuan earthquake. Yellow star shows the epicenter and white rectangles are surface projections of the ruptured faults after Furuya et al. (2010). Large circles and small triangles show stations with and without the data after the earthquake, respectively. (b) Ground projections of the IPP tracks of the LOS at the altitude 200 km (black) and 300 km (gray) from the meig station over the period 5:30-7:00 UT. Numbers close to the tracks indicate the GPS satellite numbers.

The GNSS station position time series have been used to investigate co- (Wan et al., 2017) and postseismic (Wang et al., 2021) crustal deformation, together with data from interferometric synthetic aperture radar (InSAR) (Furuya et al., 2010). Here, we use such GNSS data to study changes in ionospheric total electron content (TEC) immediately before the main shock.

Large earthquakes disturb ionosphere ~10 minutes after earthquakes when acoustic waves excited by vertical crustal movements propagate upward and reach the ionospheric F region. GNSS data are useful in studying such coseismic ionospheric disturbances (e.g., Astafyeva, 2019; Heki, 2021). Their amplitudes are especially important because they provide information on earthquake magnitudes (Cahyadi and Heki, 2015; Heki et al., 2022). For the 2008 Wenchuan earthquake, such coseismic disturbances have already been reported by Afraimovich et al (2010) and Jin et al. (2010), and we do not study them in detail here.

Here we look for anomalies immediately before the earthquake, similar to the one preceding the 2011 Tohoku-oki earthquake. Heki (2011) reported that ionospheric TEC changed its trend ~40 minutes before the mainshock, and that the areal extent of the anomaly overlaps with the fault. The finding by Heki (2011) has been criticized mainly for two reasons, i.e., inadequate distinction from space-weather origin anomalies, and ambiguity in defining reference curves to extract anomalies. The details of the criticisms and rebuttals to them before 2020 are reviewed in Heki (2021).

The debate still continues. Eisenbeis and Occhipinti (2021) pointed out dangers in arbitrarily estimating reference curves using polynomials, although the same problem has already been addressed earlier in He and Heki (2017). Ikuta et al. (2020) claimed that TEC trend changes occur more frequently than demonstrated in Heki and Enomoto (2015). However, they detected such changes mainly in low elevation satellites sensing ionosphere far from the epicenter. This is not a valid test to our hypothesis that the trend changes occur near the fault even for high elevation satellites.

Heki (2021) compiled the TEC changes before ~20 large earthquakes and found that the anomalies start earlier and grow larger for earthquake of larger magnitudes. In order to further activate the debate, it would be meaningful to add a new case, i.e., the 2008 Wenchuan earthquake, and to see its consistency with past examples.

Apart from such short-term precursory TEC changes, Liu et al. (2001) reported anomalous decrease in diurnal change amplitudes a few days prior to the 1999 Chi-chi earthquake, Taiwan. Liu et al. (2009) reported such anomalies also occurred before the 2008 Wenchuan earthquake. As an anomaly with a similar timescale, geomagnetic field changes ~3 days before the 2008 Wenchuan earthquake was also reported (Li et al., 2019). In this paper, we do not study such long-term changes, but focus on those starting immediately before the earthquake.

2.Method

2-1.GNSS Data

We use GNSS data on the day of the earthquake at 20 stations around the epicenter. However, only 6 of them recorded data over the whole day, and the remaining 14 stations stopped recording after the earthquake. The stations tracked only Global Positioning System (GPS) satellites. We removed inter-frequency satellite biases by using the values in the global ionospheric map (GIM) file, and determined the station biases using the minimum scalloping method (Rideout and Coster, 2006). After removing the biases, we converted slant TEC to vertical TEC (VTEC) by multiplying with the cosine of the incidence angle of the line-of-sight (LOS) connecting the receiver and the satellites with the hypothetical thin ionosphere at 300 km altitude.

Fig.2 shows an example of VTEC at the station meig, located ~300 km south of the epicenter. The ground tracks of the ionospheric piercing points (IPP) of LOS are given in Fig.1b. Considering that the positive electron density anomalies before the 2015 M_w8.3 Illapel earthquake emerged around altitudes ~200 km (He and Heki, 2018), we show IPP trajectories at altitude 200 km together with those at 300 km. Geomagnetic activity on this day stayed calm (Fig.S1), providing an example against the claim that large earthquakes tend to occur under high solar activity (Marchitelli et al., 2020).

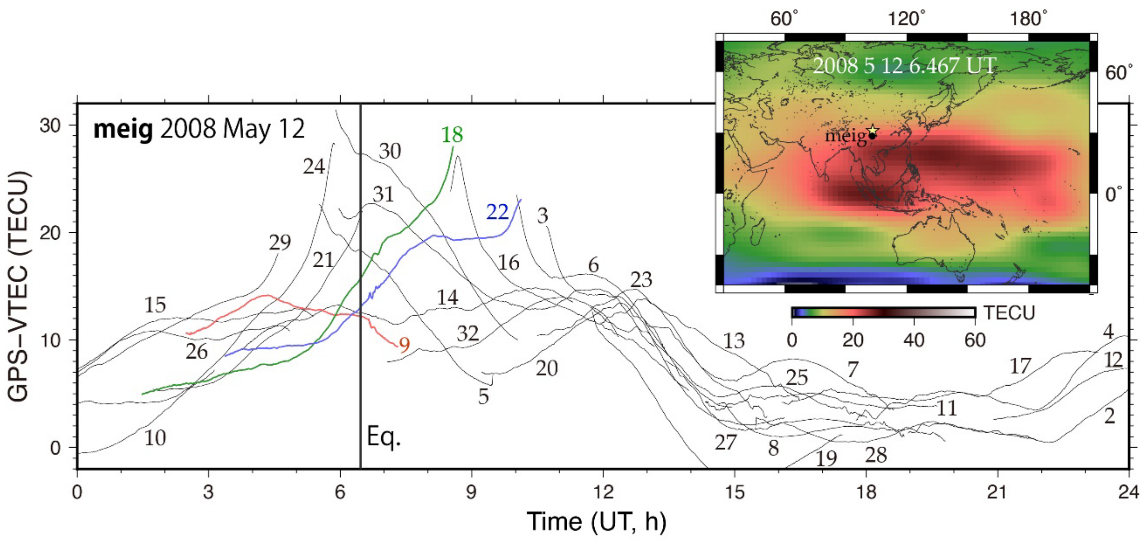

Fig. 2. VTEC on May 12, 2008, at the meig station (Fig.1a). Numbers attached to individual curves denote GPS satellite numbers. Three satellites 9, 18, 22, whose IPP tracks (Fig.1b) are relatively close to the epicenter, are shown with red, green, and blue, respectively. Solid vertical line indicates the earthquake time. The inset map shows the VTEC distribution at the time of the earthquake drawn using GIM.

The earthquake occurred shortly after the local noon. VTEC curves in Fig.2 show normal diurnal changes. Around the time of the earthquake, there are satellites with increasing and decreasing VTEC. GIM shows that the VTEC above the epicenter at the earthquake time was ~18 TECU (1 TECU = 10^{18}el/m^2). This region is located at the northern edge of the equatorial ionization anomaly, and VTEC has a strong north-south gradient (Fig.2 inset). The slopes of VTEC mainly reflect north-south gradient of the background VTEC, i.e., satellites moving southward and northward (Fig. 1b) show positive and negative slopes, respectively.

2.2 Isolation of preseismic TEC anomaly signals

In Fig.2, satellites with IPP close to the epicenter, such as the GPS satellites 18 and 22, show clear coseismic ionospheric disturbances caused by the acoustic wave arrival at the ionospheric F region ~10 minutes after earthquake. These satellites also seem to exhibit certain changes in TEC before the earthquake. From such VTEC curve, we isolate changes immediately before the earthquake using an objective procedure.

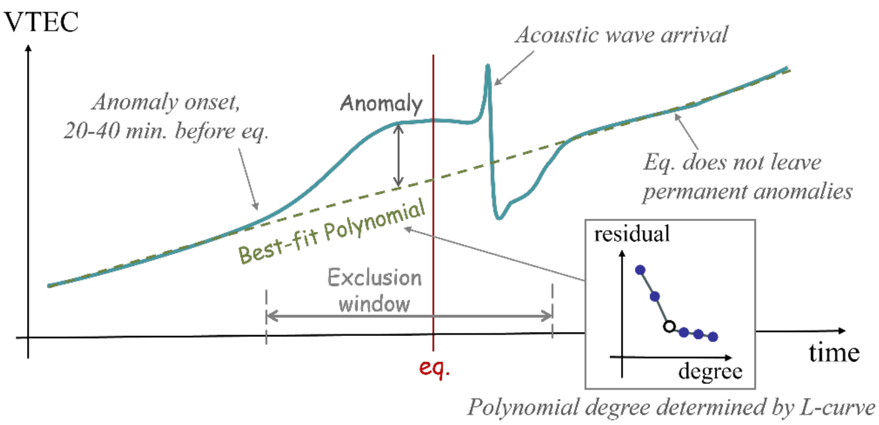

Fig. 3. We isolate TEC anomalies immediately before and after the earthquake as the departure from the reference curve estimated masking a certain window (exclusion window) as the best-fit polynomial. The reference curve depends on factors, such as degree of the polynomial, the start time, and the end time of the exclusion window. The inset shows the concept of determining the optimal polynomial degree by drawing the L-curve (the white circle shows the optimal degree).

Fig. 3 shows the procedure to extract precursory changes of ionosphere (He and Heki, 2017). First, we use the continuous VTEC data over a few hours period encompassing the earthquake time. Then, we fit a certain polynomial as the reference curve masking a certain period and consider the departure from this reference curve as the anomaly. We use data not only before but also after the earthquake to estimate the reference curve because earthquakes would not leave permanent changes in TEC, unlike station coordinates. The focus of this study is the existence of precursory signals. Hence, we do not discuss the feasibility of practical earthquake predictions.

In estimating the reference curve, we need to mask the period (exclusion window) influenced by the earthquake. The start of the exclusion window is typically 20-40 minutes before earthquake. Here, we follow Heki and Enomoto (2015) to numerically detect positive bending of the VTEC curve. By using the pair of the meig station and G09 (GPS satellite 9), we have found that the anomaly of this earthquake started ~37 minutes before earthquake (5.85 UT) (Fig.4a). The end of the window should be well after the end of the acoustic disturbances, and we set it at 7.0 UT. Fig.S2b shows that the residual curve is not so sensitive to the selection of the exclusion window.

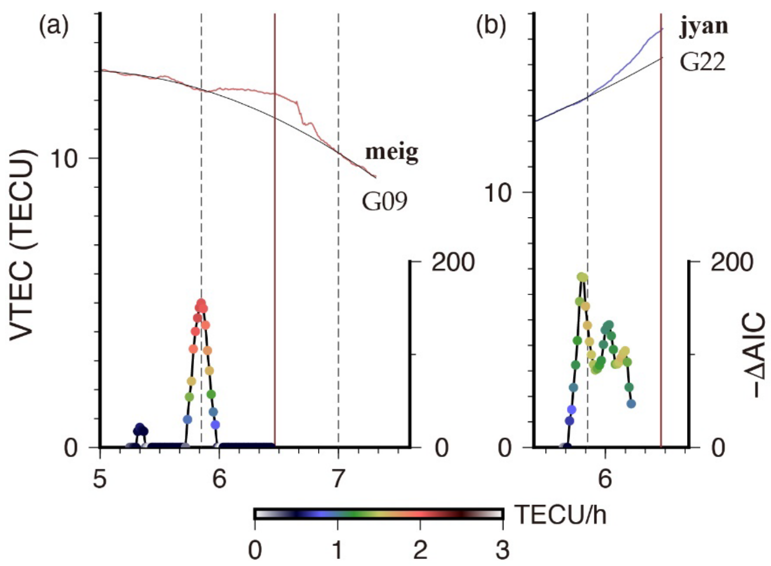

Fig. 4. VTEC curves of the meig-G09 (a) and jyan-G22 (b) pairs. We followed Heki and Enomoto (2015) to detect positive bending of these VTEC curves using the drop of Akaike's Information Criterion (AIC) by assuming a break in the middle of the 30-minutes moving window. Color of the circles attached to the AIC changes plotted at the bottom denote changes of the VTEC trends at the assumed epochs. Both cases showed significant positive bending at ~5.85 UT, used as the start of the exclusion window in subsequent calculations.

The degree of the polynomial for reference curves is determined by drawing L-curves (Fig.3 inset). It depends on the length of the period, and a longer period normally results in a higher optimal polynomial degree. Fig.S2a shows the sensitivity of the reference curve to the polynomial degree, and the L-curve suggests that the optimum degree is 2 (Fig.S2d). Fig.4 shows that the anomaly reached ~1 TECU at the time of the earthquake, which corresponds to ~5 % of the background VTEC. After the earthquake, the TEC keeps constant for ~10 minutes and decays gradually after the arrival of the acoustic disturbance.

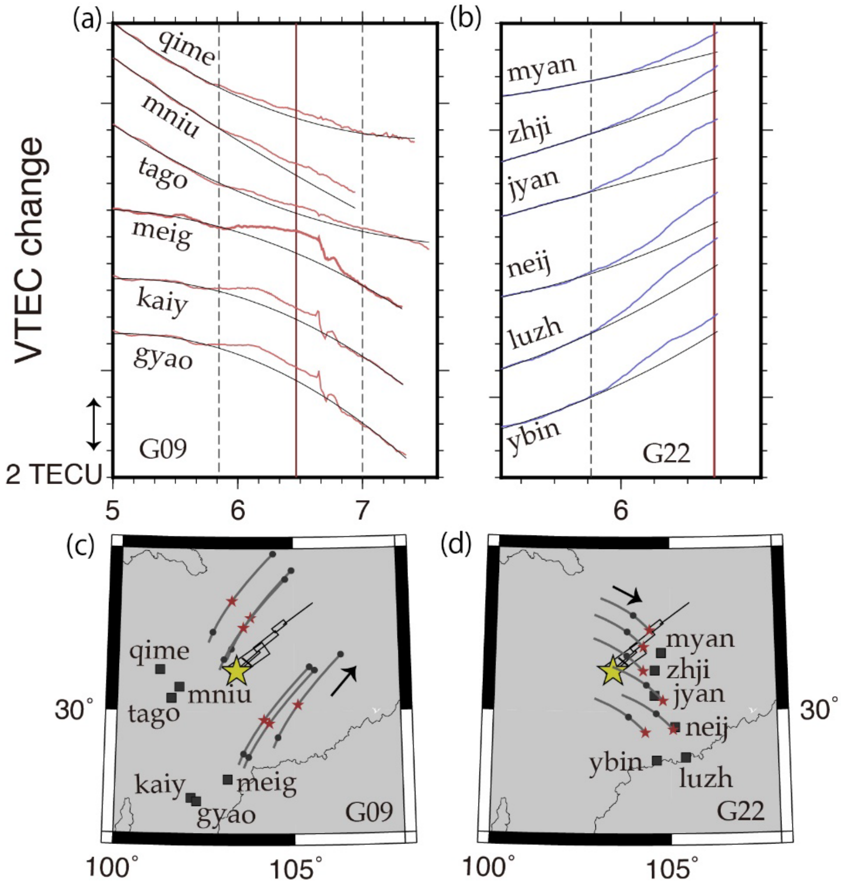

Fig. 5. VTEC change 5.0-7.4 UT with satellite G09 and six stations to the west of the epicenter without data loss (a). We used the nominal exclusion window (between the two dashed lines) and polynomial degree 2. In (b), we show the VTEC changes observed at stations to the east of the epicenter using satellite G22. We stabilized the derivation of reference curves by constraining the quadratic term around zero by ±7 TECU/hour^2 (Fig.S3) considering the absence of the postseismic data. (c) and (d) show ground projections of IPP tracks for G09 and G22, respectively, assuming a thin ionosphere at altitude 200 km.

3. Discussion

3.1 Spatial extent of the ionospheric anomaly

Next, we analyze VTEC curves from six different stations with G09 using the same exclusion window and polynomial degree (Fig.5a). The three stations with IPP to the south of the epicenter show similar TEC enhancements, while those with IPP to the north show weaker changes. This north-south asymmetry may reflect the mechanism of the generation of positive electron density anomaly, i.e., the electrons descend along the geomagnetic field being attracted by surface positive charges (Muafiry and Heki, 2020; He et al., 2022). Considering that the geomagnetic inclination at 200 km above the epicenter is ~48.6 degrees, positive electron density anomaly would elongate southward and upward along the geomagnetic field, but emerge little to the northern side of the epicenter.

In Fig.5b, we analyze VTEC curves from six different stations with G22. Because the satellite is in the western sky, we need to use stations to the east of the epicenter to see ionosphere above the epicenter. Because these stations suffer from data loss after the earthquake, we need to estimate the reference curve only with the data before the earthquake. To stabilize the estimations of reference curves, we constrained the quadratic term around zero by ±7 TECU/hour^2, optimized to realize consistency between neighboring stations (Fig. S3). One intriguing point is that the onset of the positive anomaly transfer later in the northern stations. The satellite IPP moves toward southeast, and those in early times from the northern stations were still located to the north of the epicenter.

Fig.6 compiles station-satellite pairs relatively close to the epicenter using satellites G09, G18, and G22. Because these satellites are in the northeastern, eastern, and northwestern skies, stations located to the southwestern, western, and southeastern side of the epicenter provide data at IPPs close to the epicenter. They are largely consistent with each other. Fig.6 suggests that the clear preseismic changes in ionosphere emerge within 300-400 km from the epicenter, mainly on the southern side of the epicenter.

Fig. S4 shows VTEC changes with satellite G05, G14, and G21, in the far southeastern, western, and southern skies, respectively, from six stations near the epicenter. Their IPPs are not close to the epicenter, and we do not see significant VTEC increases, for G14 and G21, immediately before the earthquake. However, G05 shows clear positive breaks of the VTEC curves synchronized with those in Fig.6. This suggests that the area showing positive change of trend immediately before the 2008 Wenchuan earthquake may extend southeastward from the ruptured faults beyond a distance of 400 km. As an alternative explanation, the positive electron density anomaly may have occurred at altitudes significantly lower than 200 km (Fig. S4a, inset map).

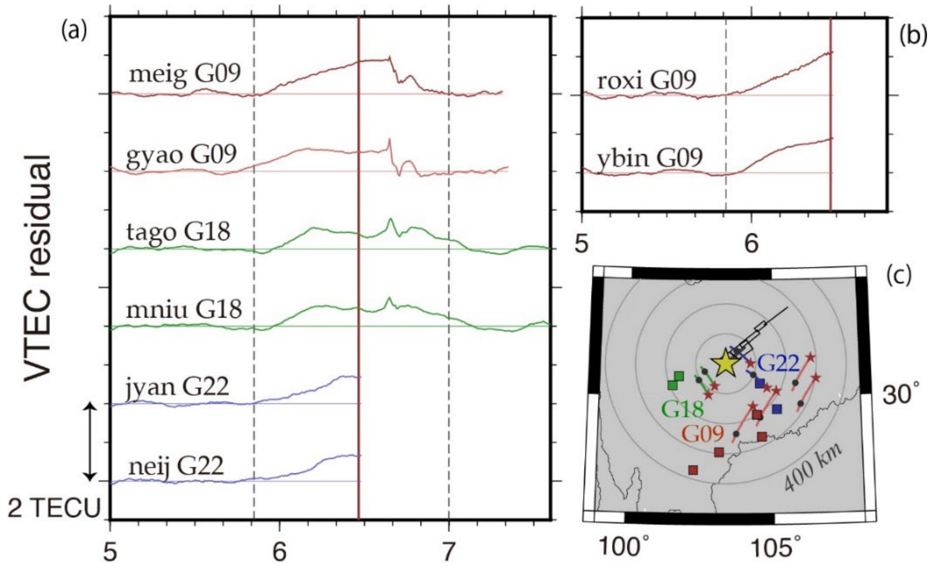

Fig. 6. VTEC residuals at 8 stations with three different satellites with various azimuths and distances from the epicenter (a, b). For the data with G18, we used the optimal polynomial degree 4 for the reference curves. The ground tracks of the 200 km IPP from 5.85 UT to the earthquake time are shown in (c).

3.2 Comparison with other earthquakes

Fig.7 compares the leading time and the intensity of the anomaly (relative to the background VTEC) with ~20 earthquakes compiled in Heki (2021). They show a simple relationship that the precursory TEC anomalies start earlier and grow stronger for earthquakes with larger M_w. This relationship reminds us of classical findings in early studies such as Scholtz et al. (1973) and Rikitake (1987). The two quantities show, however, a distinct difference in the slopes. The leading time (precursor time) scales with the power of 1/3 of the energy, while the intensity scales with the power of 2/3 of the energy. This implies that the two quantities are proportional to the length and the area of the fault, respectively.

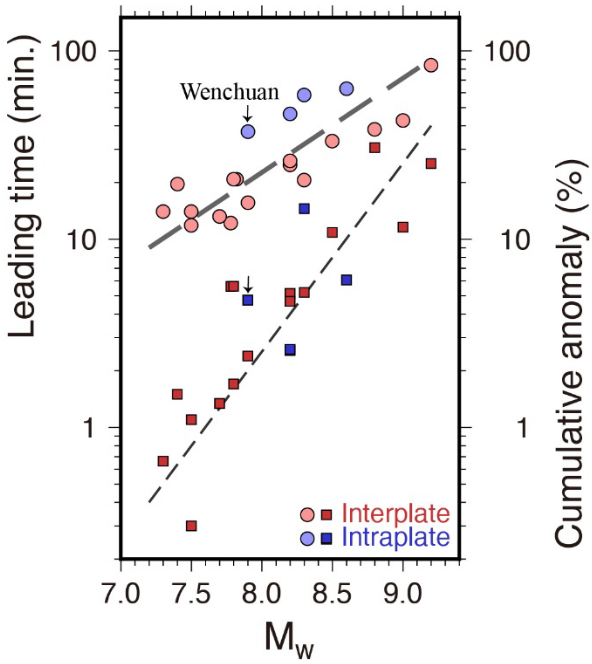

Fig. 7. Leading times (circles) and cumulative anomalies at the time of the earthquake occurrences (squares) for past earthquakes compiled by Heki (2021). Their slopes appear proportional to the power of 1/3 (thick dashed line) and 2/3 (thin dashed line) of the energy. The brand-new data of the 2008 Wenchuan earthquake (meig-G09) are marked with small arrows. Inter- and intra-plate earthquakes are discriminated using different colors.

These relationships suggest that a certain process sweeping the fault from one end to the other makes the anomaly. As hypothesized by Kelly et al. (2017) and Muafiry and Heki (2020), this process might mobilize the electric charge, and electric fields by surface charges redistribute ionospheric plasmas. Considering the similarity in time scales, this process may be linked to slow fault movements immediately before large earthquakes recently found by Bletery and Nocquet (2023).

The data of the 2008 Wenchuan earthquake are marked with arrows in Fig.7. We used the meig-G09 pair, but using other pairs in Fig.6 does not make large differences. They are consistent with the worldwide trend suggesting that the precursory changes of TEC shown in Figs.5 and 6 are typical for a M_w7.9 earthquake. This suggests that the earthquake sizes are already determined when the main ruptures start, contrary to the popular idea that earthquakes may not know their final sizes when they start (e.g., Meier et al., 2017).

The 2008 Wenchuan earthquake is an intra-plate earthquake. Their leading times (blue circles) seem somewhat longer than interplate earthquakes (red circles), although it is not clear if the differences are significant. The intensity of the precursory signals is also somewhat larger than the empirical law indicates. Considering that the 2008 Wenchuan earthquake is an inland event, its large signal may reflect the lack of loss of electric charges due to highly conductive ocean. We consider our model (Muafiry and Heki, 2020) is still highly speculative, but only the accumulation of new pieces of evidence, as presented in this article, would let it evolve toward the reality.

4. Conclusions

We analyzed the ionospheric TEC data immediately before and after the 2008 Wenchuan earthquake, China, using GNSS data from ground stations around the epicenter. They showed typical signatures immediately before large earthquakes, i.e., TEC at station-satellite pairs within a few hundreds of kilometers changed trend positively ~1/2 hour before earthquake, and the anomaly reached ~1/20 of the background VTEC. The anomaly decayed gradually after the arrival of the acoustic disturbances.

Such anomalies would not be large enough to be identified in real time before earthquakes. If the 2008 Wenchuan earthquake occurred during a high geomagnetic activity, such subtle preseismic signals would be easily blurred by disturbances of space weather origin. Nevertheless, identification of anomalies having prescribed properties would enhance the credibility of the hypothesis regarding the ionospheric anomalies immediately before large earthquakes. This study also suggests that the earthquake sizes are known when they start, which would be an important input to our understanding of earthquake generation processes.

Acknowledgements

The raw GNSS data are from the First Monitoring and Application Center, China Earthquake Administration, Tianjin. TEC information files are available from the authors upon request. GIM files were downloaded from Univ. Bern, Switzerland. We thank two anonymous referees for constructive reviews. KH is supported by President's International Fellowship Initiative of Chinese Academy of Sciences (Grant 2022VEA0014).

References

Afraimovich, E.L., Ding, F., Kiryushkin, V.V., Astafyeva, E., Jin, S., & San'kov, V. (2010), TEC response to the 2008 Wenchuan earthquake in comparison with other strong earthquakes, *Int. J. Remote Sensing*, **31** (13), 3601-3613. doi:10.1080/01431161003727747 .

Astafyeva, E. (2019), Ionospheric detection of natural hazards. *Reviews of Geophysics*, **57**(4), 1265–1288. doi:10.1029/2019RG000668

Bletery, Q. & Nocquet, J.-M. (2023), The precursory phase of large earthquakes, *Science*. **381**, 297-301.

Cahyadi, M.N. & Heki, K. (2015),Coseismic ionospheric disturbance of the large strike-slip earthquakes in North Sumatra in 2012: M_w dependence of the disturbance amplitudes, *Geophys. J. Int.*, **200**, 116-129.

Eisenbeis, J. & Occhipinti, G. (2021), The TEC enhancement before seismic events is an artifact. *J. Geophys. Res. Space Physics*, **126**, e2020JA028733, doi:10.1029/2020JA028733

Furuya, T., Kobayashi, T., Takada, Y., & Murakami, M. (2010), Fault source modeling of the 2008 Wenchuan earthquake based on ALOS/PALSAR data, *Bull. Seis. Soc. Am.*, **100**, 2750-2755, doi:10.1785/0120090242.

He, L. & Heki, K. (2017), Ionospheric anomalies immediately before Mw 7.0-8.0 earthquakes, *J. Geophys. Res. Space Phys.*,**122**, 8659–8678, doi:10.1002/2017JA024012.

He, L. & Heki, K. (2018), Three-dimensional tomography of ionospheric anomalies immediately before the 2015 Illapel earthquake, central Chile, *J. Geophys. Res. Space Phys.*,**123**, doi:10.1029/2017JA024871,

He, L., Wu, L., Heki, K. & Guo, C. (2022), The conjugated ionospheric anomalies preceding the 2011 Tohoku-Oki earthquake, Front. Earth Sci., **10**, 850078, doi:10.3389/feart.2022.850078.

Heki, K. (2011), Ionospheric electron enhancement preceding the 2011 Tohoku-Oki earthquake, *Geophys. Res. Lett.*, **38**, L17312, doi:10.1029/2011GL047908.

Heki, K. (2021), Chapter 21: Ionospheric Disturbances Related to Earthquakes in Ionospheric Dynamics and Applications, *Geophys. Monograph*, **260**, edited by C. Huang, G. Lu, Y. Zhang, and L. J. Paxton, pp.511-526, Wiley/American Geophysical Union, ISBN:978-1-119-50755-0, doi:10.1002/9781119815617.ch21.

Heki, K. & Enomoto, Y. (2015), M_w dependence of preseismic ionospheric electron enhancements, *J. Geophys. Res. Space Phys.*, **120**, 7006-7020, doi:10.1002/2014JA020223.

Heki, K., Bagiya, M.S., & Takasaka, Y. (2022), Slow fault slip signatures in coseismic ionospheric disturbances, *Geophys. Res. Lett.,* **49**, e2022GL101064, doi:10.1029/2022GL101064.

Ikuta, R., Hisada, T., Karakama, G., & Kuwano, O. (2020), Stochastic evaluation of pre-earthquake TEC enhancements, *J. Geophys. Res. Space Phys.*, **125**, e2020JA027899. doi:10.1029/2020JA027899.

Jin, S.G., Zhu, W., & Afraimovich, E. (2010), Co-seismic ionospheric and deformation signals on the 2008 magnitude 8.0 Wenchuan Earthquake from GPS observations, *Int. J. Remote Sens.*, **31**(13), 3535-3543, doi: 10.1080/01431161003727739.

Kelley, M. C., Swartz, W. E., & Heki, K. (2017), Apparent ionospheric total electron content variations prior to major earthquakes due to electric fields created by tectonic stresses, *J. Geophys. Res. Space Phys*., **122**, 6689-6695, doi:10.1002/2016JA023601.

Li, M., Yao, L., Wang, Y., Parrot, M., Hayakawa, M., Lu, J., Tan, H. & Xie, T. (2019), Anomalous phenomena in DC-ULF geomagnetic daily variation registered three days before the 12 May 2008 Wenchuan MS 8.0 earthquake. *Earth and Planetary Physics*, **3**: 330-341. doi:10.26464/epp2019034

Liu, J. Y., Chen, Y. I., Chuo, Y. J., & Tsai, H. F (2001), Variations of ionospheric total electron content during the Chi-Chi earthquake, *Geophys. Res. Lett.*, **28**, 1383-1386.

Liu, J. Y., Chen, Y. I., Chen, C. H., Liu, C. Y., Chen, C.Y., Nishihashi, M., Li, J. Z., Xia, Y. Q., Oyama, K. I., Hattori, K., & Lin, C.H (2009), Seismo-ionospheric GPS total electron content anomalies observed before the 12 May 2008 M_w7.9 Wenchuan earthquake, *J. Geophys. Res*., **114**, A04320, doi:10.1029/2008JA013698.

Marchitelli, V., Harabaglia, P., Troise, C. & De Natale, G. (2020), On the correlation between solar activity and large earthquakes worldwide, *Sci. Rep.*, **10**, 11495. doi:10.1038/s41598-020-67860-3

Meier, M. A., Ampuero, J. P., & Heaton, Th. H. (2017), The hidden simplicity of subduction megathrust earthquakes, *Science*, **357**, 1277-1281, doi:10.1126/science.aan5643.

Muafiry, I.N. & Heki, K. (2020), 3D tomography of the ionospheric anomalies immediately before and after the 2011 Tohoku-oki (M_w9.0) earthquake, *J. Geophys. Res. Space Phys*., **125**, e2020JA27993,doi:10.1029/2020JA027993.

Rideout, W., & Coster, A. (2006), Automated GPS processing for global total electron content data, *GPS Solutions*, **10**, 219–228. doi:10.1007/s10291-006-0029-5

Rikitake, T. (1987), Earthquake precursors in Japan: Precursor time and detectability. *Tectonophys.*, **136**, 265-282. doi:10.1016/0040-1951(87)90029-1

Scholz, C.H., Sykes, L.R., & Aggarwal, Y.P. (1973), Earthquake prediction: A physical basis. *Science*, **181**, 803-810, doi:10.1126/science.181.4102.803

Wan, Y., Shen, Z.-K., Bürgmann, R., Sun, J., & Wang, M. (2017). Fault geometry and slip distribution of the 2008 M_w 7.9 Wenchuan, China earthquake, inferred from GPS and InSAR measurements. *Geophysical Journal International*, **208**, 748–766. doi:10.1093/gji/ggw421

Wang, M., Shen, Z.-K. Wang, Y. Bürgmann, R., Wang, F., Zhang, P., Liao, H., Zhang, R., Wang, Q., Jiang, Z., Chen, W., Hao, M., Li, Y., Gu, T., Tao, W., Wang, K., & Xue, R. (2021). Postseismic Deformation of the 2008 Wenchuan Earthquake Illuminates Lithospheric Rheological Structure and Dynamics of Eastern Tibet. *J. Geophys. Res., Solid Earth*, **126**, e2021JB022399. doi:10.1029/2021JB022399

Xu, X., Wen, X., Yu, G., Chen, G., Klinger, Y., Hubbard, J., & Shaw, J. (2009). Coseismic reverse- and oblique-slip surface faulting generated by the 2008 Mw 7.9 Wenchuan earthquake, China.*Geology*, **37**(6), 515–518. doi:10.1130/G25462A.1

Supplementary materials

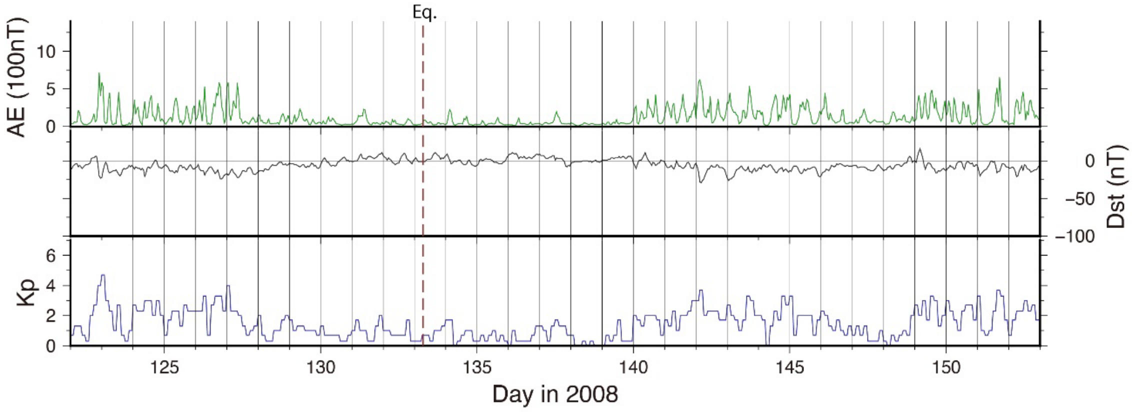

Fig. S1. Space weather indices over the whole 2008 May from NASA/Omniweb (omniweb.gsfc.nasa.gov). Geomagnetic activity was calm on the day of the earthquake (day 133).

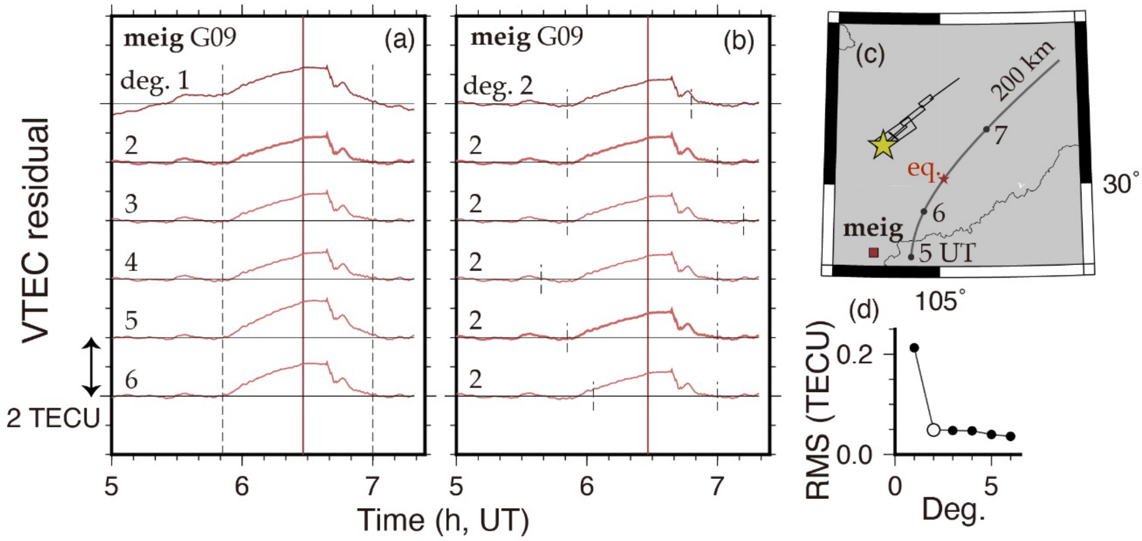

Fig. S2. VTEC residuals for the meig-G09 pair. (a) shows the residual for reference curves with different polynomial degrees. The L-curve (d) suggests that the optimal degree of the polynomial for the reference curve is 2. In (b), we compare the residuals based on reference curves estimated using different end (upper 3 curves) and start (lower 3 curves) times of the exclusion window (vertical dashed lines).

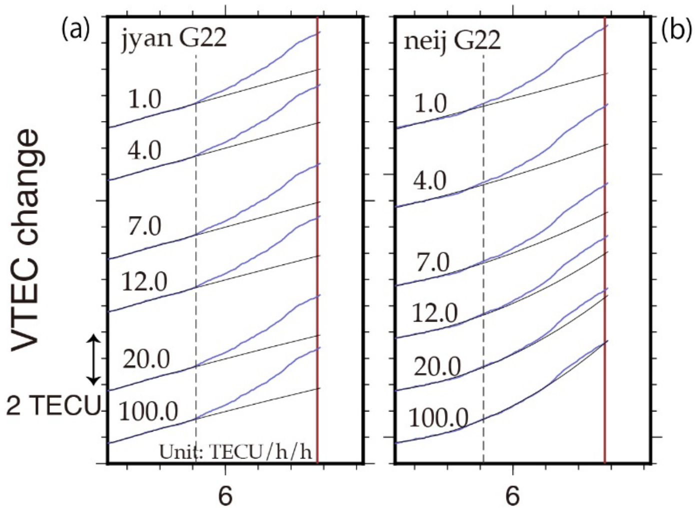

Fig. S3. Fitting quadratic functions to the part 5.0-5.9 UT and extrapolation of the curves to the earthquake time. Here we constrained the degree 2 term around zero with different tolerances attached to the curves. For the jyan station, the result is robust against the constraint, while the best-fit curve strongly depends on the constraint for the neij station. We adopt the constraint giving similar departures of the observations from the reference curves as the optimal one (±7 $TECU/hour^2$ in this case).

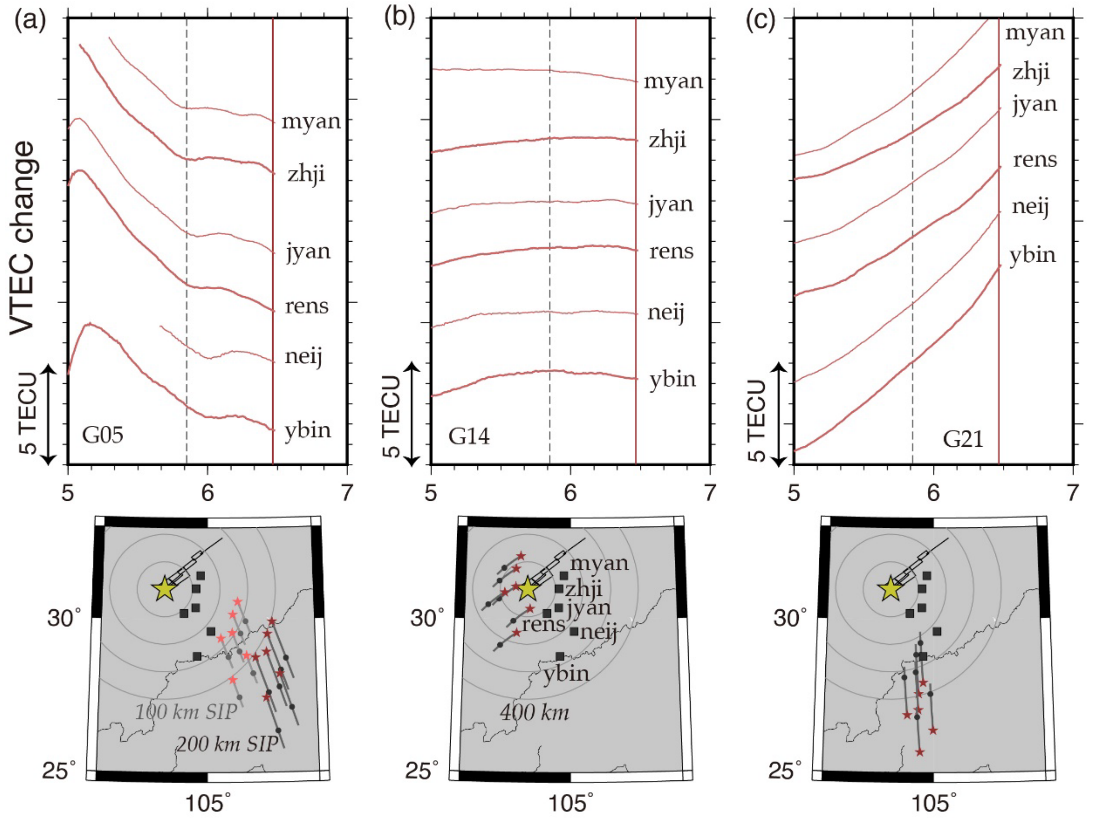

Fig. S4. VTEC curves from 5.0 UT to the earthquake time at six stations for three different satellites G05, G14, and G21 in the southeastern, western, and eastern skies, respectively. Their data are lost after the earthquakes, but we can see positive bending at the same time as in Fig. 3 for G05 satellites. However, no such bending is seen for the G14 and G21 satellites. In the map, we show 200 km IPP tracks, but we also include 100 km IPP tracks with light gray curves in (a) considering the possibility that the electron density anomaly occurs below 200 km.